CHAPTER 2

Rotor-stator Vibration Behaviour

In this chapter, a lumped-mass model for vibration of a rotor-stator system is introduced. Under the assumption of rotational symmetry, vibration solutions involving circular whirl are derived. A rotor-stator interaction model is also explained. Solutions are shown to exist involving unbalance-forced circular whirl with rub (forward whirl case) or unforced (self-excited) whirl driven by friction between the rotor and stator (backward whirl case).

2.1 Modelling Approach

2.1.1 Linear model of rotor and stator dynamics

For the system shown in figure 2.1(a), the rotor and stator each can be considered as compliantly supported masses. Circular cross-sections with uniform radial clearance between the rotor and stator may also be assumed. Prediction of vibration behaviour with rotor-stator contact interaction under the assumption of circular whirl can be based on the polar receptance method described in [9]. With the complex representation $\mathbf{z} = x + iy$, the equation describing transverse vibration of the rotor is

$$m_r\ddot{\mathbf{z}}_r + c_r\dot{\mathbf{z}}_r + k\mathbf{z}_r = De^{i\omega t} - \mathbf{p} \tag{2.1}$$

where D is a rotating unbalance force acting on the rotor and ω is the rotational frequency of the rotor. The equation of motion for the stator is

$$m_s\ddot{\mathbf{z}}_s + c_s\dot{\mathbf{z}}_s + k\mathbf{z}_s = \mathbf{p} \tag{2.2}$$

These two equations are coupled through the contact force $\mathbf{p}$.

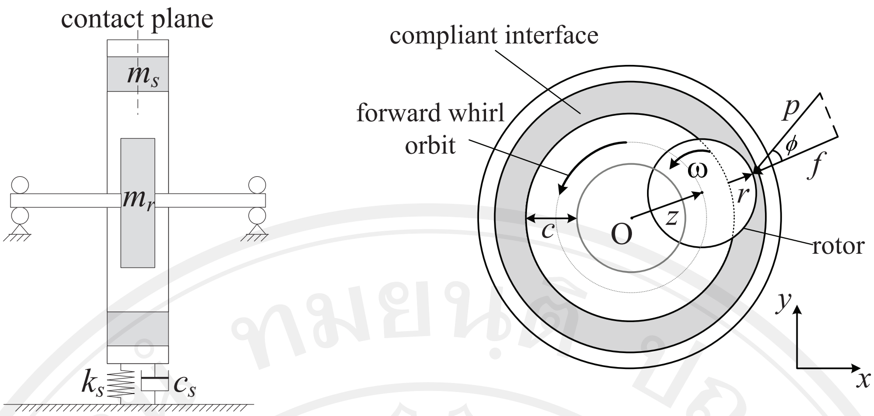

(a) Lumped-mass flexible rotor and stator model

(b) Contact geometry

Figure 2.1: Simple model for a rotor interacting with a stator

2.1.2 Nonlinear interaction Model

The geometry of rotor-stator contact across an annular clearance is shown in figure 2.1(b). Point O is the equilibrium position of the rotor center and the clearance center. When the rotor and stator are positioned at O, there is uniform radial clearance c. Here, we assume that the rotor is rigid and the stator surface is elastic. Therefore, the local contact surface of the stator is deformed in the normal direction when the contact occurs [32].

The contact interaction force $\mathbf{p} = (1+i\mu)\mathbf{f}$ will be oriented to the contact normal at friction angle $\phi = \tan^{-1}\mu$. This force makes a contact deflection (penetration) $\mathbf{r}$ in the direction of the contact normal according to a contact stiffness parameter κ. The relation between the normal contact force $\mathbf{f}$ and the contact penetration $\mathbf{r}$ is

$$\mathbf{f} = -\kappa\mathbf{r} \tag{2.3}$$

For a circular orbit, the lateral displacement vector for the rotor and the stator can be expressed $\mathbf{z}_r = \mathbf{Z}_r e^{i\omega t}$ where $\mathbf{Z}_r$ is a constant complex amplitude (and similarly for $\mathbf{z}_s$). The contact interaction force can also be written as $\mathbf{p} = \mathbf{P}e^{i\omega t}$. Using this in (2.1) and (2.2) gives equations for a steady-state response

$$(k_r - m_r\omega^2 + ic_r\omega)\mathbf{Z}_r = D - \mathbf{P} \tag{2.4}$$

$$(k_s - m_s\omega^2 + ic_s\omega)\mathbf{Z}_s = \mathbf{P} \tag{2.5}$$

Defining relative displacement $\mathbf{Z} = \mathbf{Z}_r - \mathbf{Z}_s$ then

$$\mathbf{Z} = -G(\omega)(1 + i\mu)\mathbf{F} + \mathbf{Z}_0 \tag{2.6}$$

where $G(\omega) = \frac{1}{(k_r - m_r\omega^2 + ic_r\omega)} + \frac{1}{(k_s - m_s\omega^2 + ic_s\omega)}$ is the frequency response of the combined rotor-stator system and $\mathbf{Z}_0$ is the linear response of the rotor due to unbalance force D.

Assuming, without loss of generality, that $\mathbf{Z}$ is real (zero phase). Then the contact penetration can be express $\mathbf{R} = \mathbf{Z} - c$ where c is the radial clearance. Assuming a linear force-penetration relation $\mathbf{R} = \frac{1}{\kappa}\mathbf{F}$ and using this in (2.6) gives

$$\left[(1 + i\mu)G(\omega) + \frac{1}{\kappa}\right]\mathbf{F} + c = \mathbf{Z}_0 \tag{2.7}$$

This equation allow us to make a basic prediction about when continuous circular orbits with contact are possible. The contact mode prediction will be explained further in the following section.

2.2 Prediction of Whirl with Contact

2.2.1 Forward whirl case

Consider (2.7) with substitution $\mathbf{F} = Pe^{i\phi}$, then gives

$$\left|G(\omega) + \frac{1}{\kappa}\right| Pe^{i(\phi+\psi)} + c = \mathbf{Z}_0 \tag{2.8}$$

where ψ is the phase lead of $\left(G(\omega) + \frac{1}{\kappa}\right)$ relative to $\mathbf{P}$. In forward whirl case, the possibility of sustained contact can be analysed from the vector geometry shown in figure 2.2 where $\mathbf{z}_0 = |\mathbf{Z}_0|$ assumed to be known. From the cosine rule, two possible solutions for contact force $\mathbf{P}$ are possible. For a given value of unbalance force D and whirl speed ω, a contact solution (in terms of contact force P) can be obtained as [9]

$$\frac{\|P\|}{c} = \frac{-\cos(\phi + \psi) \pm \sqrt{\cos^2(\phi + \psi) + \left(\frac{Z_0}{c}\right)^2 - 1}}{\left|G(\omega) + \frac{1}{\kappa}\right|} \tag{2.9}$$

When $Z_0 > c$ then contact between the rotor and stator cannot be avoided. There is only one positive solution for P in (2.8). The other one is negative value which can be discarded because it implies a tension between the rotor and stator. When $Z_0 < c$, the rotor can whirl without contacting the stator but sustained contact is still possible if there is a feasible solution for (2.8). Equation (2.9) shows that two real positive P solutions may exist only if $\cos(\phi+\psi) < 0$ and $\cos^2(\phi+\psi) + (\frac{Z_0}{c})^2 - 1 > 0$ as shown in figure 2.2. Consequently, it is possible to investigate the speed range that the system is unstable by using a Nyquist-type method. For any given system it is possible to determine rotational frequency at which there can be degenerated whirl responses with and without contact. If the phase of $G(\omega)$ is in range $(-\pi, 0)$, as would be expected for a passive system, then $\cos(\phi+\psi) < 0$ requires

$$\phi + \psi < -\frac{\pi}{2} \tag{2.10}$$

The requirement of $\cos^2(\phi+\psi) + (\frac{Z_0}{c})^2 - 1 > 0$ provides a minimum critical value for the non-contact whirl amplitude Z_0 that is

$$\frac{Z_0}{c} > |\sin(\phi+\psi)| \tag{2.11}$$

Accordingly, the frequency zones for sustained stator interaction may be established from a Nyquist plot of $G(\omega)$, as illustrated in figure 2.3. The frequency limits for the interaction zones follow from the intersection of the curve of $G(\omega)$ with the line originating from the

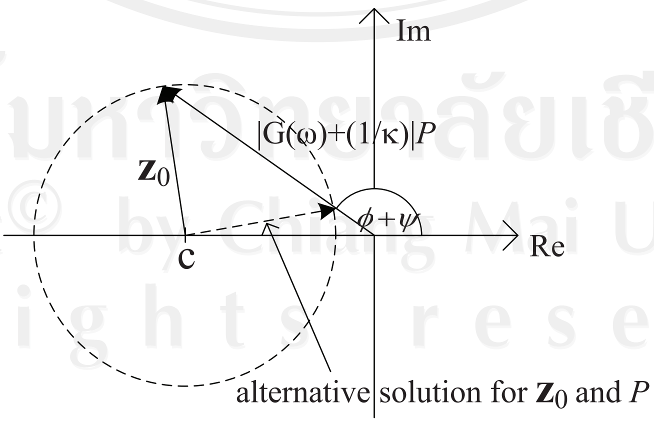

Figure 2.2: Vector geometry to analyse the contact force solution.

point $-\frac{1}{\kappa}$ with orientation $-\frac{\pi}{2} - \phi$. When rotational frequency is in the range between intersections (ω_1, ω_2), a contact-free orbit may be considered unstable in the global sense as transgression to sustained interaction is then possible, although for sufficiently small clearance or large initial orbit. Equation (2.10) and (2.11) allow, for any given system characterized by $G(\omega)$, a whirl mode map to be established showing orbit size and rotational speeds where a jump in behaviour from contact-free vibration to a sustained limit cycle vibration with rub is possible. This will be covered further in section 5.1

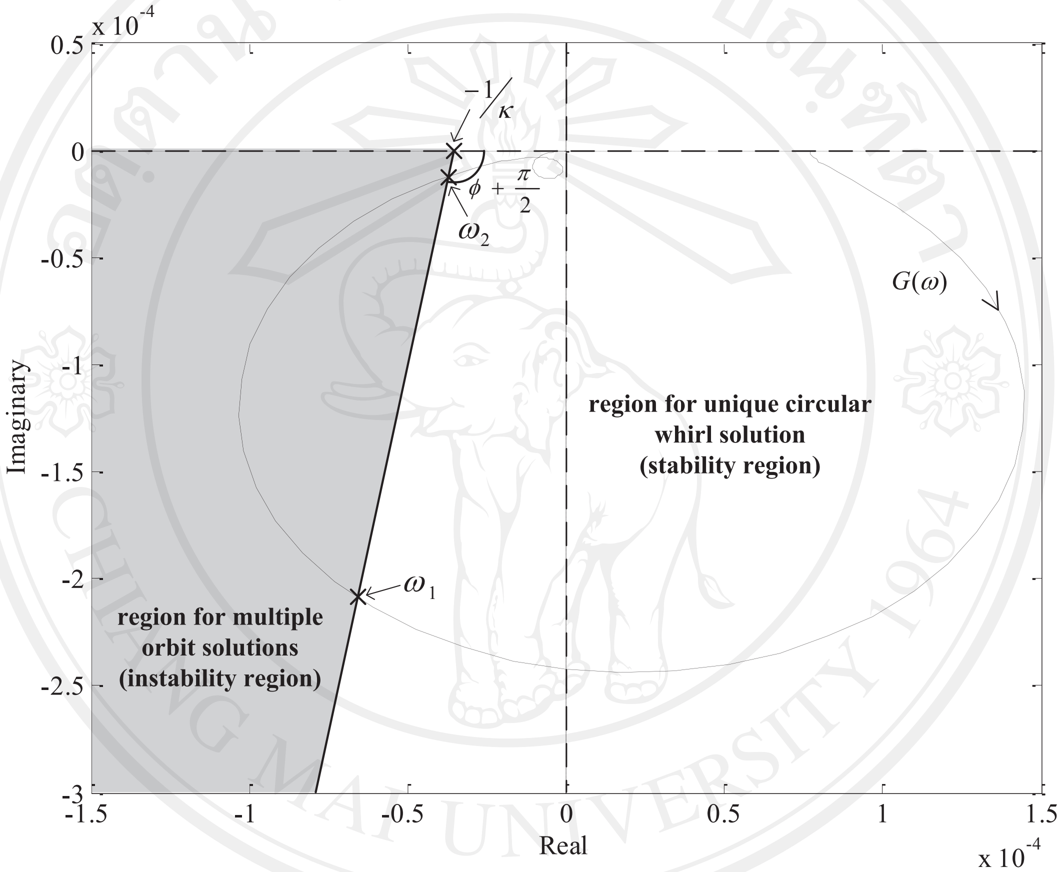

Figure 2.3: Rotational frequency zones for alternative orbit solution with rotor-stator interaction can be determined from the Nyquist plot of $G(\omega)$. Bi-stable interaction solution can exist for rotational speeds within the range $\omega_1 \rightarrow \omega_2$.

2.2.2 Backward whirl case

Backward whirl will be possible only if the friction force is sufficient to drive the whirl in a reverse direction. To analyze this case, the external disturbance is assumed to be negligible compared with the contact force ($\mathbf{Z}_0 = 0$). A backward circular orbit $\mathbf{z} = \mathbf{Z}e^{-i\Omega t}$ is then considered where Ω is the backward whirl frequency [12, 33]. Consider (2.7) with $\omega = -\Omega$ and assume for simplicity that the stator is rigidly fixed ($k_s \to \infty$) then $G(-\Omega) = \frac{1}{k_r - m_r\Omega^2 - ic\Omega}$ and (2.7) becomes

$$\left[\frac{(1+i\mu)}{k_r - m_r\Omega^2 - ic\Omega} + \frac{1}{\kappa}\right] F + c = 0 \tag{2.12}$$

Defining the natural frequency and damping ratio of the rotor as $\omega_n = \sqrt{\frac{k_r}{m_r}}$ and $\zeta_r = \frac{c_r}{2\sqrt{k_r m_r}}$ respectively, then (2.12) can be written as

$$\frac{(1+i\mu)}{1 - \left(\frac{\Omega}{\omega_n}\right)^2 - i2\zeta\left(\frac{\Omega}{\omega_n}\right)} + \frac{k_r}{\kappa} + \frac{ck_r}{F} = 0 \tag{2.13}$$

Note that the last two terms in equation (2.13) are positive real. Defining $A = \frac{k_r}{\kappa} + \frac{ck_r}{F}$ then

$$(1+i\mu) = \left[\left(\frac{\Omega}{\omega_n}\right)^2 - 1\right] A + i2\zeta A\left(\frac{\Omega}{\omega_n}\right) \tag{2.14}$$

Consider the real and imaginary parts of (2.14) :

$$\left[\left(\frac{\Omega}{\omega_n}\right)^2 - 1\right] A = 1 \tag{2.15}$$

and

$$2\zeta A\left(\frac{\Omega}{\omega_n}\right) = \mu \tag{2.16}$$

A quadratic equation comes from eliminating A from (2.15) and (2.16)

$$\left(\frac{\Omega}{\omega_n}\right)^2 - 2\frac{\zeta_r}{\mu}\left(\frac{\Omega}{\omega_n}\right) - 1 = 0 \tag{2.17}$$

The solution for (2.17) is the "backward whirl onset frequency" [12, 34]

$$\frac{\Omega}{\omega_n} = \frac{\zeta_r}{\mu} + \sqrt{\left(\frac{\zeta_r}{\mu}\right)^2 + 1} \tag{2.18}$$

Considering the definition of parameter A and (2.16) then

$$\frac{k_r}{\kappa} + \frac{ck_r}{F} = \frac{\mu}{2\zeta_r}\left(\frac{\omega_n}{\Omega}\right) \tag{2.19}$$

Thus, for positive value of contact force F.

$$\frac{k_r}{\kappa} < \frac{\mu}{2\zeta_r}\left(\frac{\omega_n}{\Omega}\right) \tag{2.20}$$

The condition for existence of the positive solution F to (2.13) is thus given by [33]

$$\frac{\kappa}{k_r} > 2\left(\frac{\zeta_r}{\mu}\right)^2\left[1+\sqrt{1+\left(\frac{\mu}{\zeta_r}\right)^2}\right] \tag{2.21}$$

This condition implies that the required friction level for backwards whirl increases as the contact stiffness κ decreases or the level of rotor damping is increased. The maximum value of κ for non-existence of backward whirl solution has been calculated for a range of friction coefficient values and the corresponding boundary for possibility of backward whirl solution is shown in figure 2.4

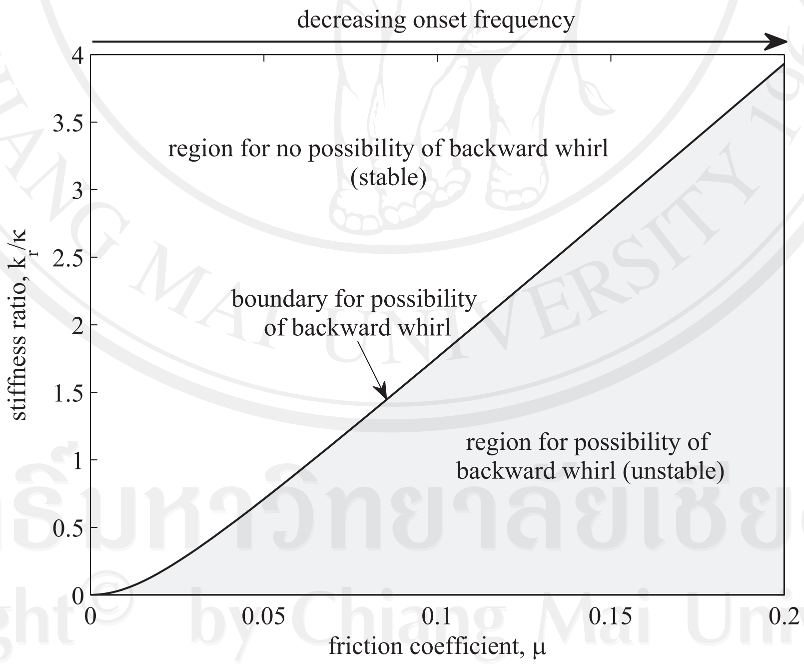

Figure 2.4: Boundary for possibility of a backward whirl solution can be determined from condition (2.21)

2.3 Example of Whirl Prediction with Contact

Model-based prediction of possible amplitude jump and dry friction backward whirl with rotor-stator interaction in a single transverse plane are further considered for a specific case. To demonstrate how to apply prediction theory to a realistic case, a flexible rotor system model is introduced and shown schematically in figure 2.5. The rotor has a mass of 0.5 kg mounted on a flexible shaft of length 1 m supported by ball bearings at both ends. For lateral vibration of the rotor, the natural frequency corresponding to the first flexural mode is 310 rad/s. The stiffness and damping ratio of the rotor mid-span are 48 kN/m and 0.087 respectively. The stator is modeled as a compliantly supported lumped mass of 0.8 kg at the mid-span location with natural frequency of vibration 1,118 rad/s and damping ratio 0.023. The radial clearance between the rotor and stator at contact plane is 0.3 mm.

2.3.1 Forward whirl case

In this subsection, friction is not included in the rotor system model. The combined rotor-stator frequency response $G(\omega)$ is shown in the Nyquist plot (figure 2.6). For a given bound on the nonlinear contact stiffness for rotor-stator interaction κ, the complex plane is divided into two regions by a vertical line through the point $-1/\kappa$. For illustration, the case that κ is 40 kN/m is shown ($1/\kappa = 2.5 \times 10^{-5}$ m/N). At rotational frequency ω for which $G(\omega)$ falls to the right side of the line, only one possible circular orbit solution exists. Otherwise, more than one orbit solution is possible. Note that the largest loop in

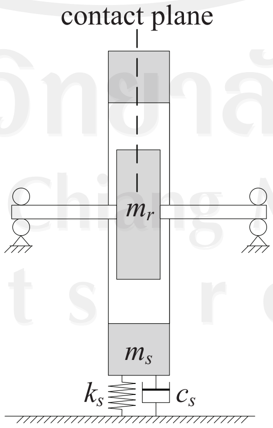

Figure 2.5: A flexible rotor and stator model.

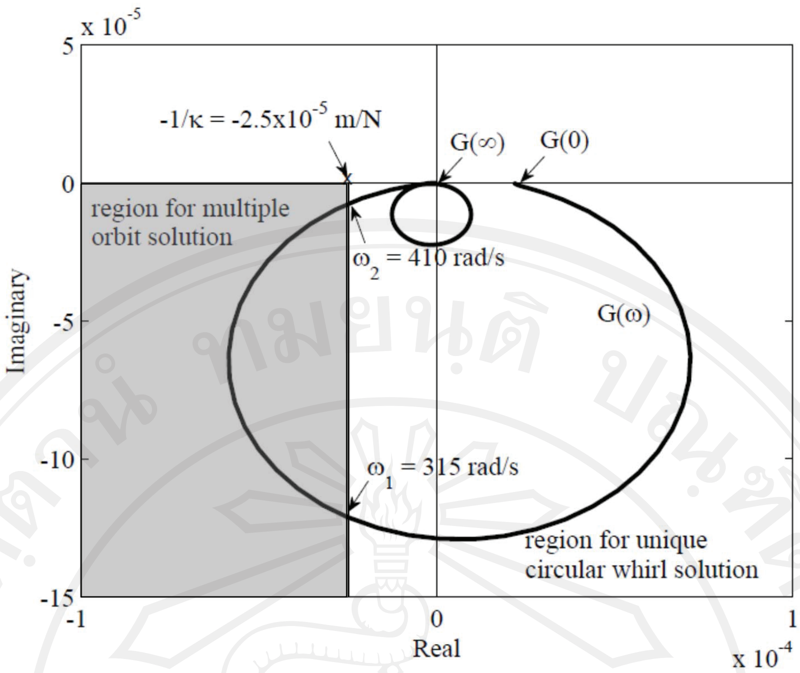

Figure 2.6: Alternative orbit solution with rotor-stator interaction exists for rotational frequency within the range 315 to 410 rad/s.

$G(\omega)$ occurs for frequency values close to the natural frequency of the rotor. For this case, the potential for amplitude jump is indicated for rotational frequencies in the range 315 to 410 rad/s. This does not imply that amplitude jump can occur for any nominal orbit but only one for which $|Z_0|$ is sufficiently large so that

$$|Z_0| > c|\sin(\phi + \psi)| \tag{2.22}$$

For the rotor system presented in this example, $|Z_0|$ has to be less than 0.245 mm. in order to avoid amplitude jump.

Consider the case when the rotor is operated at frequency of 280 rad/s. $G(280)$ falls to the right side of the shaded region in figure 2.6 and this implies that an amplitude jump cannot happen. This prediction has been confirmed by simulation, as shown in figure 2.7. This figure shows transient response of the rotor due to temporary step change in disturbance, d_x. The initial vibration of the rotor is within the clearance space and there is no contact with the stator. When amplitude of disturbance is suddenly increased, vibration of the rotor exceeds the clearance space and then there is a contact between the rotor and stator. However, the contact interaction ceases when the disturbance returns back to the original level.

When $G(\omega)$ falls to the left side region and equation (2.22) is satisfied, amplitude jump behaviour can be possible. A simulated case where the rotor is operated at frequency of 345 rad/s is shown in figure 2.8. In this case, the contact between the rotor and stator persists after the disturbance returns back to the original level. Thus, it is confirmed that two possible vibration behaviours (one with contact and one without) can occur for this operating condition, in terms of rotational speed and unbalance.

This example illustrates how to use a Nyquist plot to predict the potential for amplitude jump. The prediction is confirmed by the simulation of the transient response of the rotor system due to a temporary step change in disturbance.An example of backward whirl prediction is shown in the following subsection.

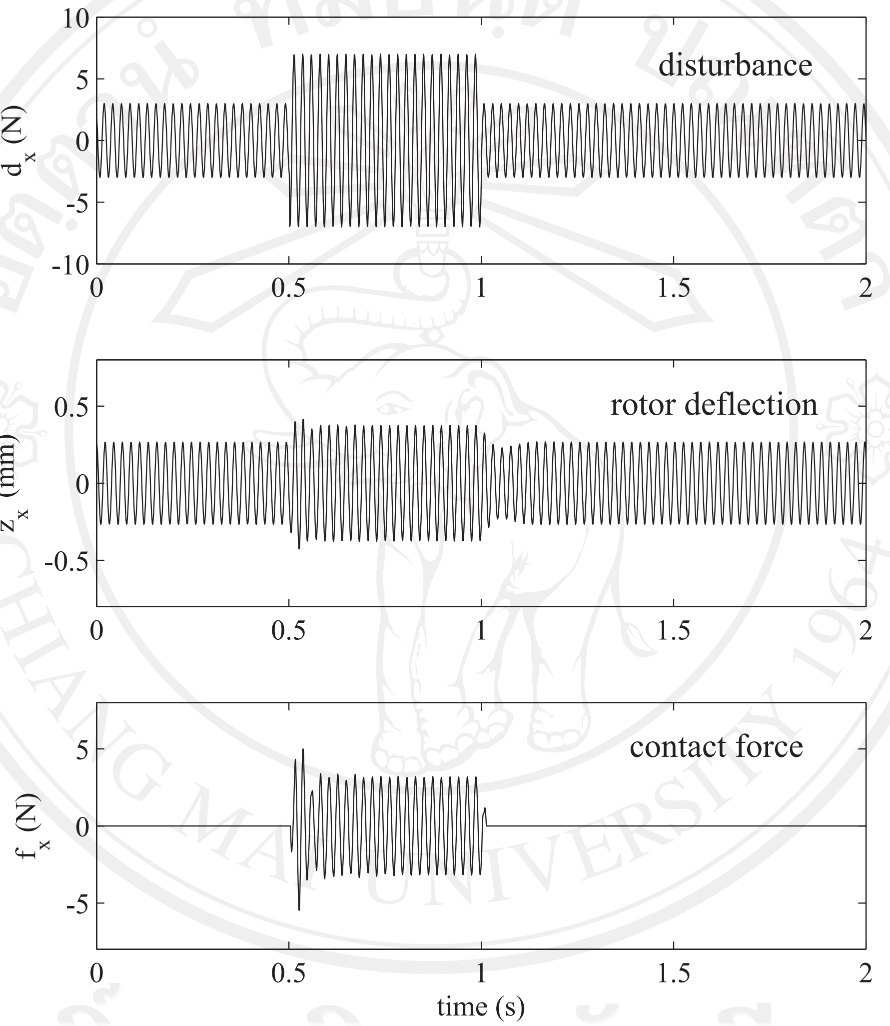

Figure 2.7: Transient response of the rotor system due to temporary step change in disturbance at operating frequency of 280 rad/s

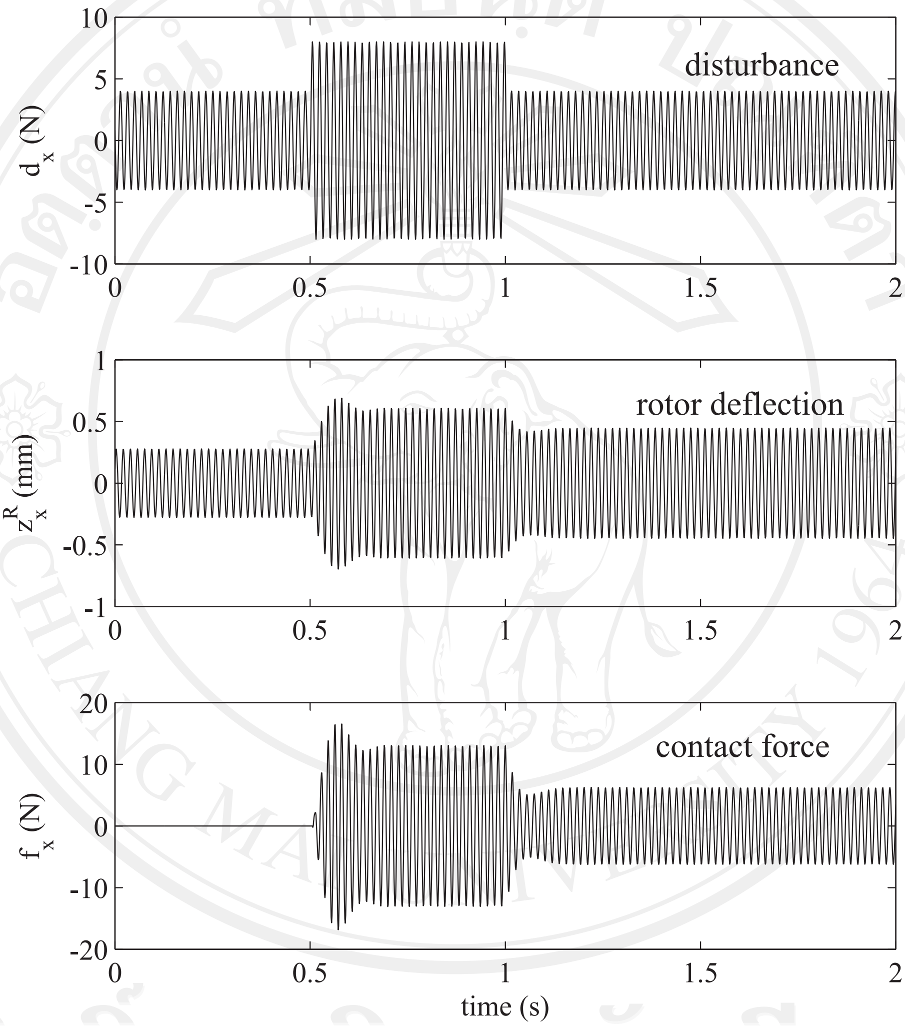

Figure 2.8: Transient response of the rotor system due to temporary step change in disturbance at operating frequency of 345 rad/s

2.3.2 Backward whirl case

In this subsection, the method for prediction of backward whirl solutions is presented for a specific case. Friction between the rotor and stator at a contact plane is now accounted for in the model of section 2.1. Typically, a friction coefficient between dry steel surfaces is approximately 0.5 [35]. Figure 2.9 shows a boundary for existence of backward whirl solution (gray region) which is calculated from (2.21) for a range of friction coefficient from 0 to 1. The stiffness ratio, k_r/κ, for the rotor model presented in this example is 1.2. Two different values of friction coefficient at point A and B are selected as examples in order to show the influence of friction on the possible vibration behaviours.

For point A in figure 2.9, the friction coefficient value of 0.1 is considered and this also was used for simulation. From the predicted boundary in figure 2.9, the backward whirl solution does not exist for this point. A simulation results for transient response is shown in figure 2.10. A step change in sinusoidal disturbance induces contact between the rotor and stator. The development of the rotor orbit is shown in figure 2.11. The initial orbit of the rotor is in a contact-free level as shown in figure 2.11a. Increasing of the disturbance causes the rotor to contact with the stator (figure 2.11b). Friction between the rotor and stator surfaces has little influence on the rotor response and the orbit is still in the pattern of full annular rub (figure 2.11c).

The friction coefficient for point B in figure 2.9 is 0.5 and this point is seen to indicate a potential for a backward whirl response (see figure 2.9). The simulation for this case was undertaken and is shown in figure 2.12. Contact begins after 0.5 seconds and the vibration of the rotor grows in an unstable manner. Figure 2.13 shows how the rotor orbit develops from a contact-free orbit to a fully-developed backward whirl. Initially, the rotor is whirling in a contact-free level (figure 2.13a) and then a disturbance is increased in order to get the rotor-stator contact. At this point, the rotor orbit is in a pattern of bouncing motion because the friction force tends to drive the rotor to whirl in the reverse direction to rotation (figure 2.13b). As the bouncing increases in severity, the rotor orbit develops to become more backwards in character (figure 2.13c) and this progresses to a fully-developed backward whirl as seen in figure 2.13d.

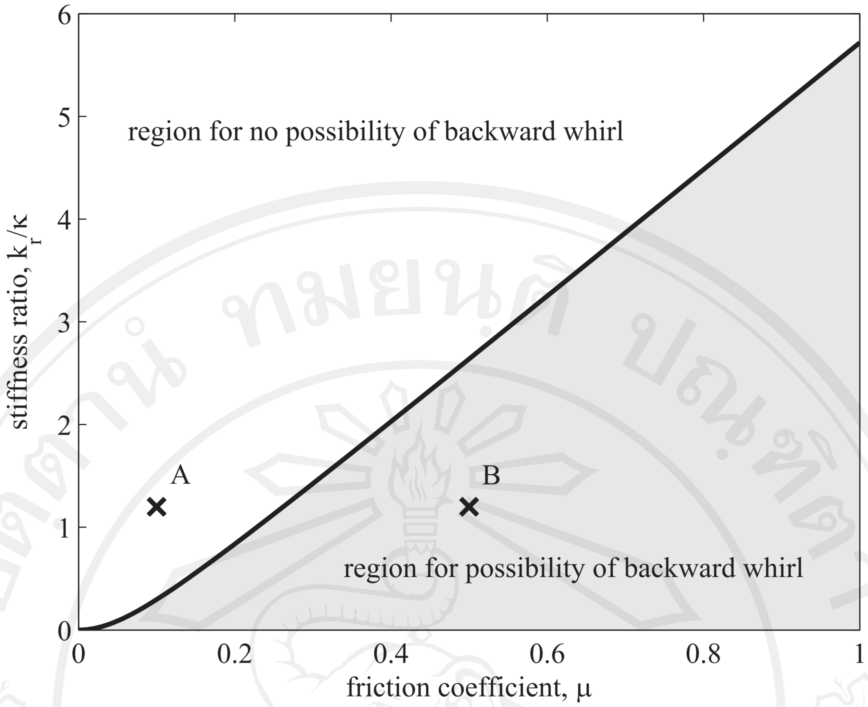

Figure 2.9: Boundary for possibility of backward whirl solution of the rotor system at operating frequency of 280 rad/s

This example illustrates the basic idea to calculate and predict the region for potential of backward whirl from equation 2.21. The simulation and the orbit plots show the rotor orbit development from a contact free level to a fully develop backward whirl.

2.4 Summary

A simple non-linear interaction model for rotor-stator vibration has been introduced where the contact between rotor and stator is assumed to be possible in one plane. Basic prediction methods for unstable response behaviour involving forward whirl and backward whirl have been explained. The conditions for existence of rub solutions were obtained under assumptions of rotational symmetry. Examples of whirl prediction with contact were shown in order to investigate how unstable response behaviour of the coupled rotor-stator system could be predicted numerically.

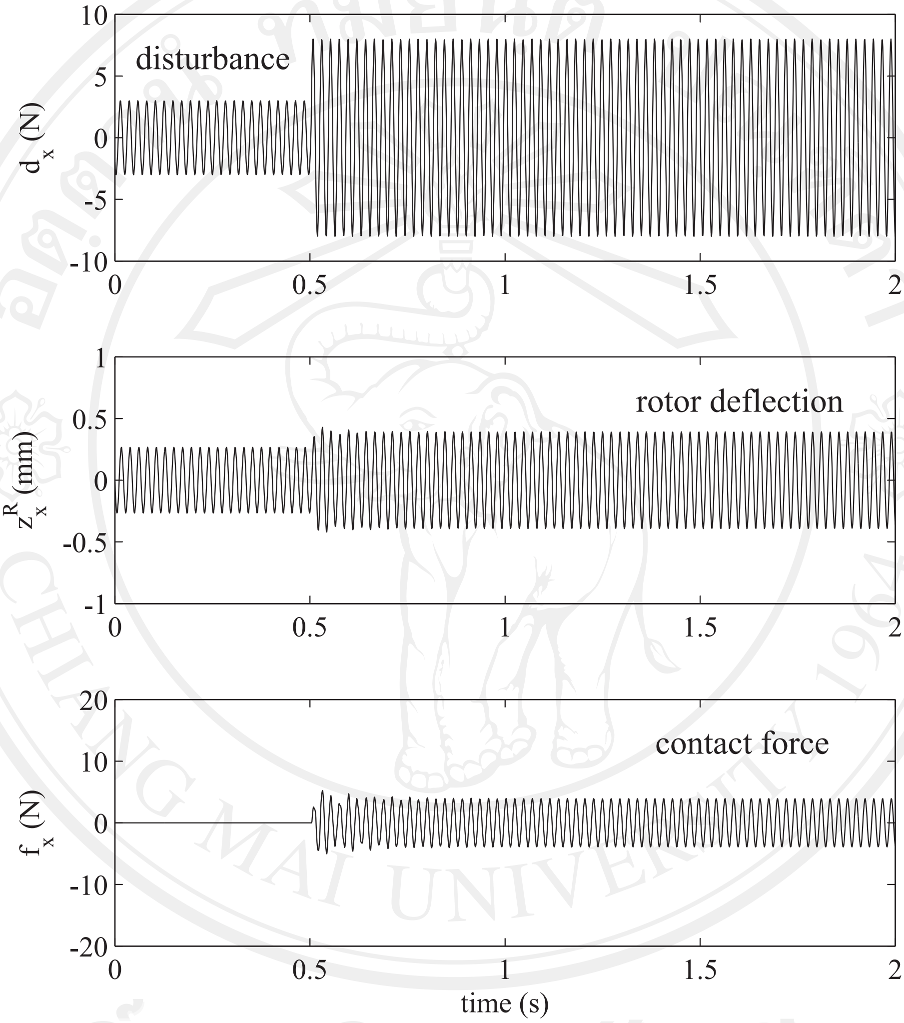

Figure 2.10: Transient response of the rotor system (with friction coefficient for rotor and stator surfaces $\mu = 0.1$) due to step change in disturbance at operating frequency of 280 rad/s

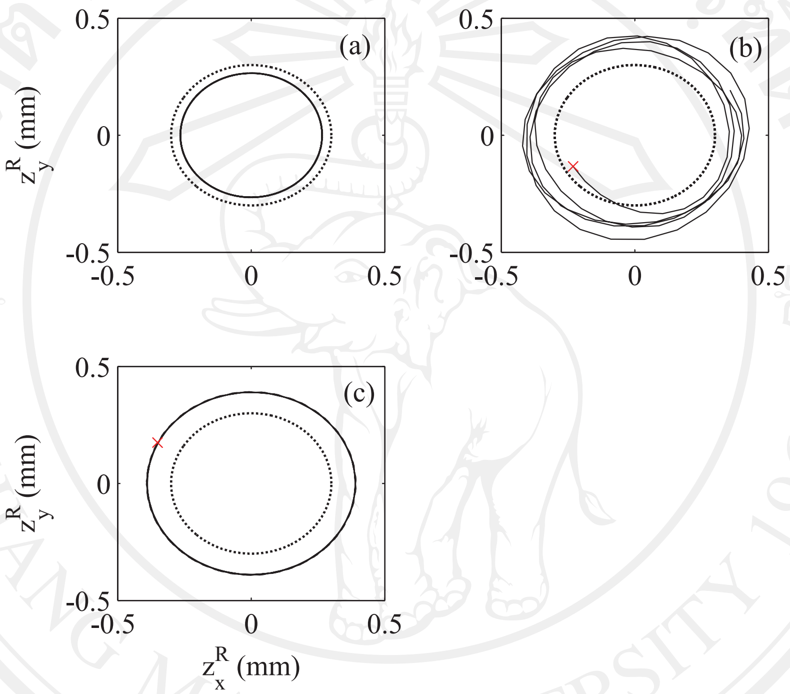

Figure 2.11: Orbit plots of the rotor at operating frequency of 280 rad/s with friction coefficient for rotor-stator surfaces $\mu = 0.1$ (a) initial contact free orbit (b) rotor-stator rubbing transition orbit (c) rotor whirl with full annular rub. An initial limit of clearance is indicated by a dot circle.

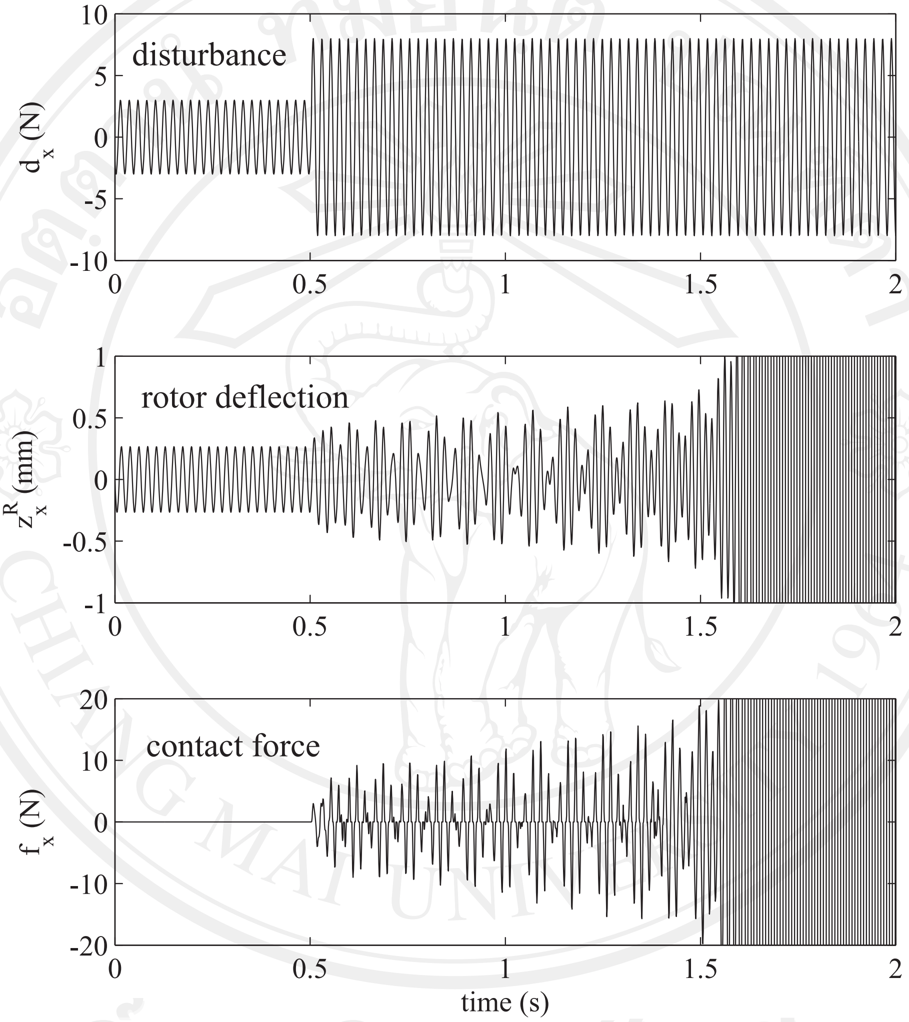

Figure 2.12: Transient response of the rotor system (with friction coefficient for rotor and stator surfaces $\mu = 0.5$) due to step change in disturbance at operating frequency of 280 rad/s

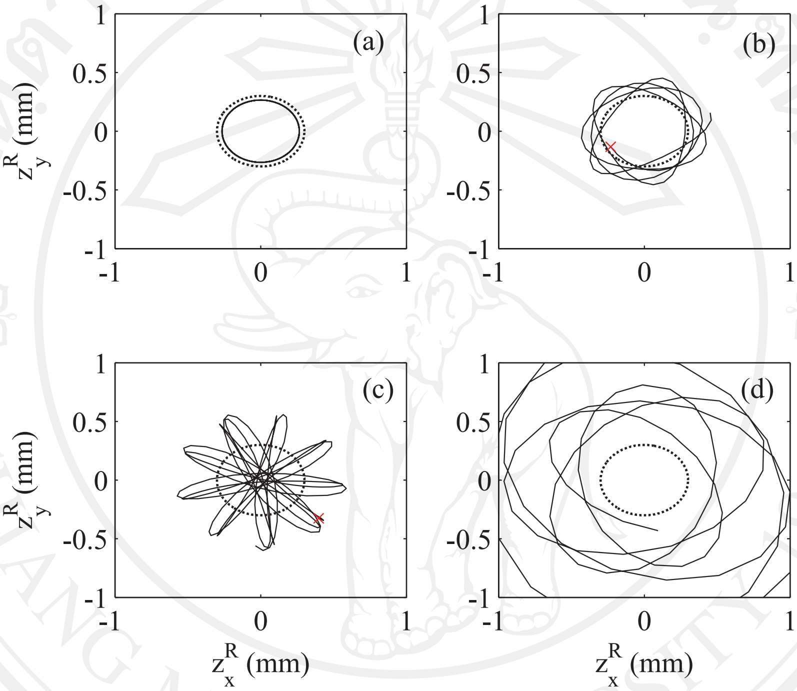

Figure 2.13: Orbit plots of the rotor at operating frequency of 280 rad/s with friction coefficient for rotor-stator surfaces $\mu = 0.5$ (a) initial contact free orbit (b) rotor-stator rubbing transition orbit (c) rotor orbit is developed to friction driven backward bouncing (d) instability orbit of friction driven backward whirl. An initial limit of clearance is indicated by a dot circle.